J Braz. Soc. Mech. Sci. Eng. (2015) 37:1405–1416
DOI 10.1007/s40430-014-0247-7

TECHNICAL PAPER

Effect of swirl on performance and emissions of CI engine in HCCI mode

T. Karthikeya Sharma · G. Amba Prasad Rao · K. Madhu Murthy

Received: 17 July 2014 / Accepted: 6 September 2014 / Published online: 12 October 2014

Abstract A promising combustion strategy that combines the advantages of both SI and CI combustion modes is the homogeneous charge compression ignition (HCCI) combustion mode. A volumetric combustion of a lean mixture of charge is the advantage of HCCI combustion, leading to low NO_x emissions and soot. In this work, HCCI combustion mode is analyzed to study the effect of swirl motion of intake charge on performance and emissions of the engine using a Three-Zone Extended Coherent Flame Combustion Model (ECFM-3Z, Compression Ignition). The present study revealed that ECFM-3Z of STAR-CD predicts well the in-cylinder pressures, temperatures, cylinder wall heat transfer losses, piston work and emissions such as CO, CO_2 and NO_x of the CI engine in the HCCI mode. The ECFM-3Z model has a predicted variation in turbulent kinetic energy and velocity magnitudes inside the cylinder during combustion, facilitating better understanding of the combustion process. The simulation results show that the there is a reduction in in-cylinder peak pressures and temperatures, as the swirl increases and CO emissions increase because of reduced temperatures, and CO_2 and NO_x emissions decrease because of the reduced in-cylinder temperatures. It is found that there is a trade-off between the emissions and piston work. Higher turbulent energy and velocity magnitude levels are obtained with increase in swirl, indicating efficient combustion without a demanding combustion chamber design.

Keywords HCCI engine · ECFM-3Z · Swirl motion · Emissions and performance

1 Introduction

IC Engines have become indispensible prime movers over the past one-and-a-half century. Though the performance of conventional SI and CI engines is satisfactory, SI engine suffers from poor part load efficiency and high CO emissions. The CI engine yields high particulate and NO_x emissions. These effects may be attributed to their conventional combustion process. Of late, a hybrid combustion process called homogeneous charge compression ignition (HCCI) equipped with advanced low-temperature combustion technology has been gaining attention from researchers. In principle, HCCI involves the volumetric auto-combustion of a premixed fuel, air and diluents at low to moderate temperatures and at high compression ratios. The other associated advantages with HCCI mode of combustion have been well documented and presented as a potentially promising combustion mode for internal combustion engines [1, 2].

The different combustion models which are well developed for predicting engine processes are transient interactive flamelets (TIF) model, digital analysis of reaction system–transient interactive flamelets model (DARS–TIF), G-equation model, extended coherent flame combustion model—3 zones [3, 4] and the equilibrium-limited ECFM (ECFM-CLEH) [5, 6]. Each model has its own limitations and is suitable for a specific set of problems. Generally speaking;

Technical Editor: Luis Fernando Figueira da Silva.

T. Karthikeya Sharma (✉) · G. Amba Prasad Rao · K. Madhu Murthy
Department of Mechanical Engineering, National Institute of Technology Warangal, 506004 Hanamkonda, Telangana, India
e-mail: karthikeya.sharma3@gmail.com

G. Amba Prasad Rao
e-mail: gap@nitw.ac.in

K. Madhu Murthy
e-mail: madhu@nitw.ac.in

Table 1 Combustion model capabilities

Model	Applicability
G-Equation	Partially premixed SI and CI
DARS-TIF	Compression ignition
ECFM	Non-homogeneous premixed SI
ECFM-3Z	Premixed and non-premixed SI and CI

ECFM-3Z and ECFM-CLEH can be used for all types of combustion regimes, whereas ECFM-3Z is mostly suitable for homogeneous turbulent premixed combustion with spark ignition and compression ignition. The applicability of various combustion models is shown in Table 1. Owing to its wide applicability, in the present work ECFM-3Z has been used to study the effect of swirl motion of intake charge on emissions and performance of the HCCI engine.

Induction-induced swirl has a predominant effect on mixture formation and rapid spreading of the flame front in the conventional combustion process of a CI engine. This has been well documented in the literature. However, it is observed that no work has been done on the effect of swirl in the HCCI mode. The present study is concerned with the analysis of engine-pertinent performance parameters by varying the swirl intensity and its effect on the emissions and performance of a CI engine in the HCCI mode. For this purpose, four swirl ratios between 1 and 4, both inclusive, were chosen. The analysis is aimed at studying parameters such as in-cylinder pressures, temperatures and cylinder wall heat transfer losses; emissions including CO, CO_2 and NO_x; and piston work, turbulent kinetic energy and velocity magnitude. The present study emphasizes on maximizing the piston work and minimizing the NO_x emissions, and accordingly the respective optimum swirl ratios are arrived at for the chosen engine configuration.

2 Methodology

A single-cylinder direct injection, reentrant piston bowl CI engine with specifications given in Table 2 is considered for the analysis. A CFD package STAR-CD is used for the analysis to study the heat release rates, in-cylinder pressures and temperatures, and CO and NO emissions were modeled in CI engine HCCI mode. The engine specifications considered for the analysis are shown in Table 2. The analysis was done from the second cycle after the engine was started.

3 CFD model setup

The piston bowl shape and 3D mesh of the piston bowl sector are shown in Fig. 1. The computational mesh consists

Table 2 Engine specifications

Engine specifications	
Displacement volume	1,600 cm^3
Bore	12.065 cm
Stroke	14 cm
Connecting rod length	26 cm
Compression ratio	21:1
Fuel	n-Dodecane
Operating conditions	
Engine speed	1,000 rpm
Equivalence ratio	0.26
Inlet temperature air (T_{air})	353 K
Inlet air pressure (P_{air})	0.1 MPa
Cylinder wall temperature (T_{wall})	450 K
EGR	0 %

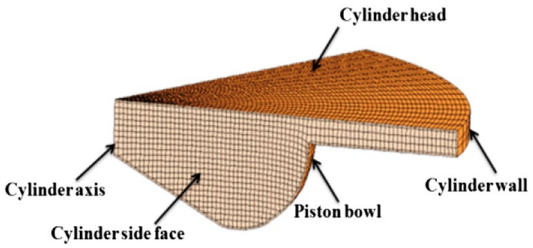

Fig. 1 Schematic representation of 3D piston bowl shape at TDC

of 0.312×10^6 cells. The entire mesh consists of a cylinder and 1/6th of a piston bowl created in Hypermesh—a mesh generation utility—and is imported into STAR-CD for solutions. A spline was developed based on the imported model; a 2D template was cut by the spline to cut the 3D mesh with 60 radial cells, 160 axial cells, 5 top dead center layers and 40 axial block cells.

The energy efficiency of the engine is analyzed by the gross indicated work per cycle (*W)* calculated from the cylinder pressure and piston displacement using Eq. (1):

$$W(\mathrm{Nm}) = \frac{\pi a B_2}{8} \int_{\theta_1}^{\theta_2} p(\theta) \left[2\sin(\theta) \frac{a\sin(2\theta)}{\sqrt{l^2 - a^2 \sin^2(\theta)}} \right] d\theta, \tag{1}$$

where a, l and B are the crank radius, connecting rod length and cylinder bore, respectively, and θ_1 and θ_2 are the beginning and the end of the valve-closing period.

The indicated power per cylinder (P) is related to the indicated work per cycle using Eq. (2):

$$P(\mathrm{kW}) = \frac{WN}{60,000 n_R}, \tag{2}$$

where $n_R = 2$ is the number of crank revolutions for each power stroke per cylinder and N is the engine speed (rpm).

The indicated specific fuel consumption (ISFC) is shown in Eq. (3):

$$\mathrm{ISFC}\left(\mathrm{g}/\mathrm{kWh}\right) = \frac{30\mathrm{m}_{\mathrm{fuel}}N}{P}. \tag{3}$$

In Eq. (1), the power and ISFC analyses can be viewed as being only qualitative rather than quantitative in this study.

4 Modeling strategy

The STAR-CD used in the present study has integrated several sub-models such as turbulence, fuel spray and atomization, wall function, ignition, combustion, NO_x and soot models for various types of combustion modes in CI as well as SI engine computations. As the initial values of k and ε are not known a priori, the turbulence initialization is done using the I–L model. For this purpose, the local turbulence intensity, I, and length scale, L, are related as:

$$k_\infty = 3/2\, I^2 V_\infty^2 \tag{4}$$

$$(\varepsilon_\infty = C_\mu^{3/4} k_\infty^{3/2}/L). \tag{5}$$

This practice will ensure that k and ε and the turbulent viscosity μ_t, will all scale correctly with V_∞, which is desirable from both the physical realism and numerical stability point of view. Moreover, the turbulent intensity is defined using the same velocity vector magnitude as stagnation quantities.

The combustion is modeled using ECFM-3Z. As far as fluid properties are concerned, ideal gas law and temperature-dependent constant pressure specific heat (C_p) are chosen.

4.1 Swirl creation

In this section, swirl motion is created by changing the velocities of the intake charge in the U and V directions. The U and V components of the velocity are calculated with the code using the formulae shown:

$$U = -(x - x_{\mathrm{CSYS}})\,(\mathrm{Swirl.\ RPM}.2\pi)/60 \tag{6}$$

$$V = -(y - y_{\mathrm{CSYS}})\,(\mathrm{Swirl.\ RPM}.2\pi)/60 \tag{7}$$

where U and V are the velocity components of the intake charge in the X and Y directions. RPM represents the speed of the engine. x, x_{CSYS}, y, y_{CSYS} represents the global and local coordinates of x and y, respectively. The z coordinates of the global and local coordinates were matched during modeling and after meshing, to eliminate the errors in swirl creation.

4.2 Spray injection and atomization model

In conventional CI mode, spray and atomization are modeled using Huh's model [7, 8]. Huh's model considers the two most important mechanisms in spray atomization: gas inertia and the internal turbulence stresses generated in the nozzle. The agitation of jet takes place because of turbulence generated in the nozzle when it exits the hole. Surface wave growth takes place once the agitation of the jet reaches a certain limit leading to droplet formation.

The secondary breakup of the droplets is modeled by considering the Reitz–Diwakar model [9, 10]. The Reitz–Diwakar model incorporates the droplet breakup due to non-uniform pressure surrounding the droplet (bag breakup) and the other is because of continuous phase (stripping breakup). The occurrence of these regimes is dependent on the magnitude of the droplet incidence Weber number (We_d) and the dimensionless droplet diameter d^* as shown in Eq. (8):

$$We_d = \frac{\rho_d D_d V_{d,n}^2}{\sigma}, \tag{8}$$

where 'n' is the unit normal to the wall, '$V_{d,n}$' is the normal component of droplet velocity relative to the wall and 'σ' is the surface tension coefficient.

For HCCI combustion mode, the premixed reaction mechanism is adopted for the homogeneous fuel air mixture formation.

4.3 Autoignition model

Ignition delay is computed to establish the ignition occurrence time, instead of the pre-ignition kinetics.

The autoignition delay τ_d calculated based on semi-empirical correlations is shown in Eq. (9):

$$\tau_d = 1.051\times10^{-8}[\mathrm{F}]^{0.05}\left[\mathrm{O}_2\right]^{-0.53}\rho^{0.13}\mathrm{e}^{5914/\mathrm{T}\mu}[47/\mathrm{CN}], \tag{9}$$

where CN is the cetane number (max = 60). An ignition progress variable function defined to track the development of the reactions prior to autoignition is shown in Eq. (10):

$$\left(\mathrm{d}Y_{\mathrm{igi}}\right)/(\mathrm{d}t) = Y_{\mathrm{Tf}}F(\tau_d). \tag{10}$$

For HCCI combustion mode, a double delay autoignition model is used, as the autoignition in HCCI mode is controlled by the effect of cool flames. In the cool flame regime, the rise in temperature is less and the reaction rates are slowed down. After the second delay, the reaction rates increase leading to main autoignition.

Double-delay autoignition considers two delay times and two ignition progress variables. The delay times are not empirical correlations, but are obtained from precomputed tables, which can also provide the information about the maximum fuel burned at each autoignition step.

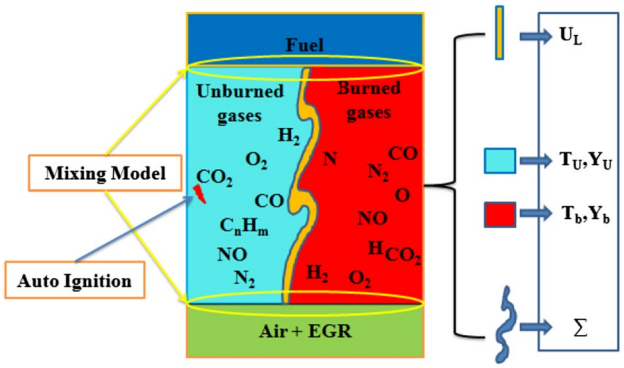

Fig. 2 Schematic representation of three zones of the ECFM-3Z model

4.4 Combustion model

A three-zone extended coherent flame combustion model (EFCM-3Z) is used for the analysis. A premixed charge with autoignition was considered for the start of combustion. In the HCCI engine, the air fuel mixture enters the cylinder as in SI engines, and combustion occurs by compression ignition as in CI engines. Figure 2 depicts the schematic representation of the three zones of the ECFM-3Z model. This model is capable of simulating complex mechanisms such as turbulent mixing, flame propagation, diffusion combustion and pollutant emission that characterize modern IC engines.

For the combustion analysis of CI engine in conventional mode, turbulent mixing, flame propagation, diffusion combustion models and post-flame emission models were used. For HCCI mode mixing model, post-flame emissions model and double-delay autoignition models were used.

For wall-bounded flows, most turbulence is generated in the near-wall region. It is therefore necessary to resolve the details of the near-wall flow, which in turn requires a fine mesh in that region. For this, the Angelberger wall function model is used [11].

The mixed zone is the result of turbulent + molecular mixing between gases in the other two zones, where combustion takes place.

The other two zones are characterized by the fuel in the unmixed fuel zone and the species in the unmixed air + EGR zone.

The equations governing the mass fractions of the unmixed fuel (Y_{fum}) are shown as:

$$\frac{\partial \rho Y_{\text{fum}}}{\partial t} + \nabla \cdot (\rho u Y_{\text{fum}}) - \nabla \cdot \left[\left(D + \frac{\mu_t}{SC_t} \right) \nabla Y_{\text{fum}} \right] = \frac{\beta_{m_{in}}}{\pi} Y_{\text{fum}} \left(1 - Y_{\text{fum}} \frac{\rho}{\rho_u} \frac{w_m}{w_f} \right) + \dot{\omega}_e \text{Vap}. \tag{11}$$

4.5 NO_x model

The high temperatures during the combustion process facilitate the formation of nitrous oxides consisting of NO_2 and NO due to the reaction between atmospheric nitrogen and oxygen. NO_x emissions are highly affected by the temperature. The higher the combustion temperatures, the higher will be the formation of NO_x. There are two possible sources of nitrous oxide formation in engines, namely, thermal and prompt NO_x. In diesel engines, however, more than 90 % of the NO emission stem from the thermal NO formation process. The current approach to modeling NO production is with the extended Zel'dovich mechanism [12]. The extended Zel'dovich mechanism consists of the following equations as described by Bowman [12]:

$$O + N_2 \leftrightarrow NO + N \tag{12}$$

$$N + O_2 \leftrightarrow NO + O \tag{13}$$

$$N + OH \leftrightarrow NO + H. \tag{14}$$

With the partial equilibrium of Eq. (14) for the hydrogen radicals,

$$O + OH \leftrightarrow O_2 + H. \tag{15}$$

The extended Zeldovich mechanism can be written as a single rate equation for NO, as originally put forth by Heywood [13] and shown in Eq. (14):

$$\frac{\mathrm{d}}{\mathrm{d}t}[NO] = 2k_{1f}[O][N_2] \left\{ \frac{\left\{ 1 - [NO]^2 / K_{12}[o_2] \Sigma \mathrm{d}_2 \right\}}{1 + k_{1b}[NO] / \left(k_{2f}[o_2] + k_{3f}[OH] \right)} \right\}, \tag{16}$$

where $K_{12} = (k_{1f}/k_{1b})(k_{2f}/k_{2b})$ and the subscripts 1, 2 and 3 refer to Eqs. (12), (13) and (14), respectively. O, OH, O_2 and N_2 are assumed to be in local thermodynamic equilibrium.

4.6 Soot modeling

Soot formation is the most common process that can be observed during the combustion of fuel-rich hydrocarbons. Fuel pyrolysis and oxidation, formations of polycyclic and aromatic hydrocarbons, and the inception of first particles are the complex reactions that are involved in the formation of soot. A laminar flamelet model where the scalar quantities are related to scalar dissipation rates and mixture fractions, developed by Karlson et al. [14], is used to model the soot. Karlson developed a correlation between the rate of soot formation with premixed counterflow flames and local conditions in diffusion flames. In this method, an additional transport equation for the soot mass fraction is solved. Integration of mass fraction space with probability density

function is made to get the soot volume fraction source term from the flamelet library. To save computer memory and CPU time, the flamelet library of sources is constructed using a multiparameter fitting procedure, resulting in a proper simple algebraic set of parameters. The transport equation for soot mass fraction is shown in Eq. (17):

$$\frac{\partial}{\partial t}(\rho Y_s) + \frac{\partial}{\partial x_j}(\rho u_j Y_s) = \frac{\partial}{\partial x_j}\left(\frac{\mu_t \partial Y_s}{\mathrm{Pr}_{t,S}\,\partial x_j}\right) + \rho_s \bar{\omega}_v, \tag{17}$$

where *Ys* is the soot fraction. The Prandtl number for soot is assumed to be 1.3 and the soot density $\rho_s = 1{,}860\ \mathrm{kg/m^3}$.

$$\bar{\omega}_{v,i} = \alpha_i \int_0^{\alpha}\int_0^{1} \frac{1}{f_v}\left(\frac{\partial f_{v,i}}{\partial t}\left(\hat{f},\hat{\chi}\right)\right) P\left(\hat{f},\hat{\chi}\right) d\hat{f}\, d\hat{\chi} \tag{18}$$

$i = s_{\mathrm{g,fr,OX}}$, where $x\hat{}$ is the scalar dissipation rate. In the above equation, s_g stands for surface growth, fr for fragmentation, ox for oxidation and α_i are the scaling factors corresponding to each of these effects. They enable the user to scale the rates up or down for sensitivity studies or calibration purposes.

4.7 EGR modeling

Exhaust gas recirculation is mainly used to reduce NO_x emissions and improve autoignition. There are two EGR models as stated below.

(a) Variable composition—this model considers the components present in the EGR mixture. In this model, up to six EGR scalars are defined, namely EGR_O2, EGR_CO2, EGR_CO, EGR_H2O, EGR_H2 and EGR_N2. These scalars are then solved by transport equations. The EGR_O2 scalar does not take part in the reaction.
(b) Fixed composition—the EGR composition is defined by entering values for each component's mass fraction in the O2, CO2, H2O, N2, CO and H2 boxes. The sum of the supplied values must be equal to 1.0.

In the present analysis, the variable composition model is used. In this model it is considered as the mass of the recirculating exhaust gas (m_{egr}) divided by the total mass that enters the cylinder (m_{I}).

Thus,

$$\mathrm{egr} = \frac{m_{egr}}{m_I}, \tag{19}$$

where

$$m_{\mathrm{I}} = m_{\mathrm{air}} + m_{\mathrm{egr}} + m_{\mathrm{f}}. \tag{20}$$

For the individual species,

$$m_{\mathrm{egr(f)}} = \mathrm{egr}.\, m_{\mathrm{E(f)}} \tag{21}$$

$$m_{\mathrm{egr(O_2)}} = \mathrm{egr}.\, m_{\mathrm{E(O_2)}} \tag{22}$$

$$m_{\mathrm{egr(CO_2)}} = \mathrm{egr}.\, m_{\mathrm{E(CO_2)}} \tag{23}$$

$$m_{\mathrm{egr(N_2)}} = \mathrm{egr}.\, m_{\mathrm{E(N_2)}} \tag{24}$$

$$m_{\mathrm{egr(H_2O)}} = \mathrm{egr}.\, m_{\mathrm{E(H_2O)}}, \tag{25}$$

where "m_{f}" is the mass of the fuel.

Subsequently, the mass fractions can be determined by dividing the mass of each individual exhaust gas by the total mass of all exhaust gases.

5 Initial and boundary conditions

The simulation is started with an absolute pressure of 1.02 bar, 0 % EGR, temperature 353 K and equivalence ratio 0.26 are taken as initial values. Fixed boundary wall temperatures are taken with combustion dome regions of 450 K, piston crown regions of 450 K and cylinder wall regions of 400 K. The Angelberger wall function mode [15] is considered. In the 'two-layer' and low Reynolds number approaches, no-slip conditions are applied directly and the boundary layers are computed by solving the mass, momentum and turbulence equations (the latter in their 'low Reynolds number' form) within them. The hybrid wall boundary condition which is a combination of two-layered and low Reynolds number wall boundary conditions is considered in this analysis. This hybrid wall boundary condition removes the burden of having to ensure a small enough near-wall value for y^+ (by creating a sufficiently fine mesh next to the wall). The y^+ independency of the hybrid wall condition is achieved using either an asymptotic expression valid for $0.1 < y^+ < 100$ or by blending low Reynolds and high Reynolds number expressions for shear stress, thermal energy and chemical species wall fluxes. This treatment provides valid boundary conditions for momentum, turbulence, energy and species variables for a wide range of near-wall mesh densities.

Standard wall functions are used to calculate the variables at the near-wall cells and the corresponding quantities on the wall. The initial conditions were specified at IVC, consisting of a quiescent flow field at pressure and temperature for full load condition.

6 Validation of ECFM-3Z, compression ignition model

STAR-CD is a well-known commercial CFD package adopted by many renowned researchers and well-established research organizations in the field of automotive IC engines. The results obtained through this package are validated with the experimental results of many authors, such as Pasupathy

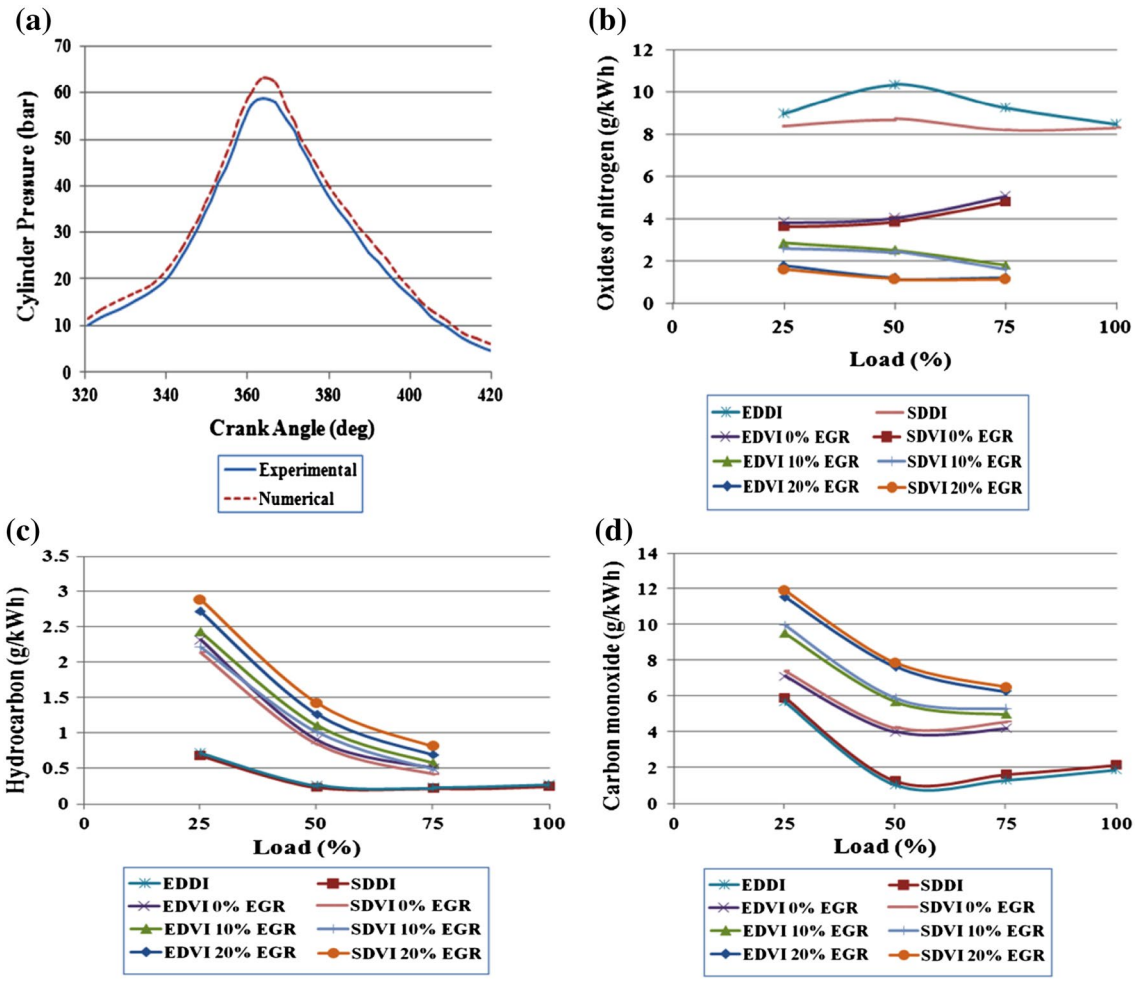

Fig. 3 Validation of the ECFM-3Z compression ignition model with the experimental results of external mixture formation of the HCCI engine

Venkateswaran et al. [16], Zellat Marc et al. [17] and Bakhshan et al. [18]. A comparison of the CI engine in HCCI was done in this paper considering the extended coherent flame combustion three zones compression model for combustion analysis. The present paper deals with the simulation of the CI engine in the HCCI mode, using a fuel vaporizer to achieve excellent HCCI combustion in a single-cylinder air-cooled direct injection diesel engine. No modifications were made to the combustion system. Ganesh et al. [19] conducted experiments with diesel vapor induction without EGR and with 0, 10 and 20 % EGR. Validation of the present model with the experimental results of Ganesh et al. [19] was done by considering all the engine specifications.

In their study, vaporized diesel fuel was allowed to mix with air to form a homogeneous mixture and inducted into the cylinder during the intake stroke. To control the early ignition of diesel vapor–air mixture, cooled (30 °C) exhaust gas recirculation (EGR) technique was adopted. Figure 3 represents validation of simulated results with the experimental results of Ganesh et al. [19]. It is observed that the simulated results are in good agreement with the experimental results. The comparison of the plots between simulation and experimental results are shown in Fig. 3. In the figures, EDVI represents the experimental diesel vapor injection and SDVI represents simulated diesel vapor induction at the respective EGR concentrations.

7 Results and discussion

In the present paper, the effect of swirl motion on the performance of HCCI engine with diesel as fuel was studied with swirl ratios ranging from 1 to 4. Analysis of the effect of swirl ratio on a single-cylinder HCCI engine was simulated, using a three-zone extended coherent flame (ECFM-3Z) CFD model. The results are plotted and discussed below.

7.1 In-cylinder pressures

The variation of in-cylinder pressures with swirl ratios is plotted in Fig. 4. It can be seen that there is a marginal

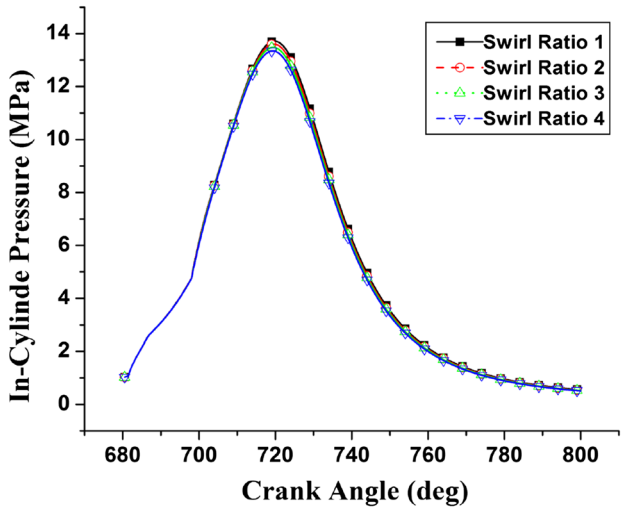

Fig. 4 In-cylinder pressure vs crank angle

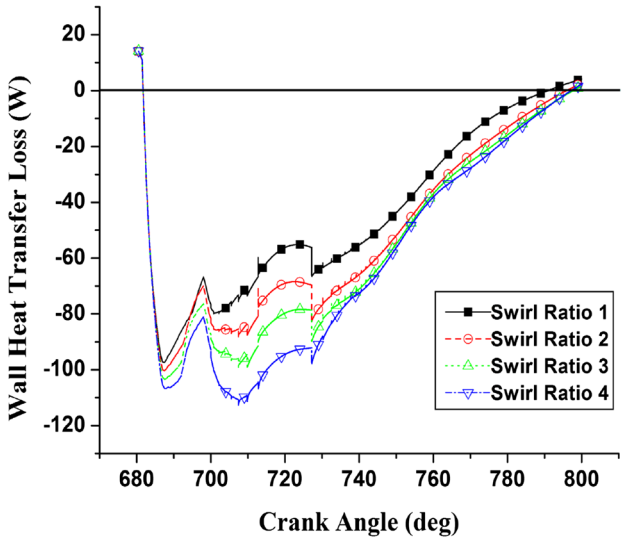

Fig. 5 Wall heat transfer loss vs crank angle

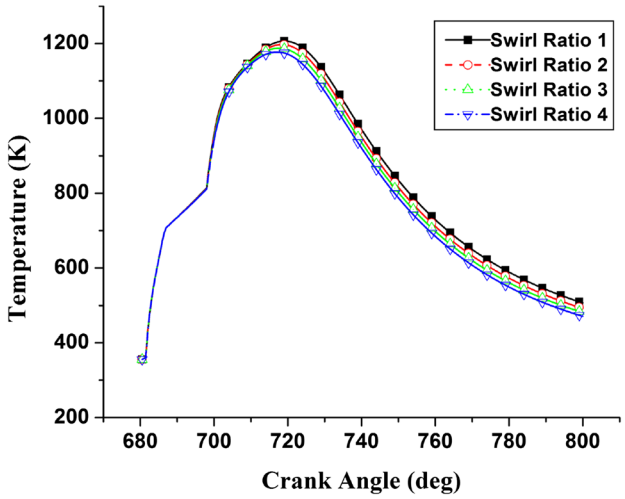

Fig. 6 Temperature vs. crank angle

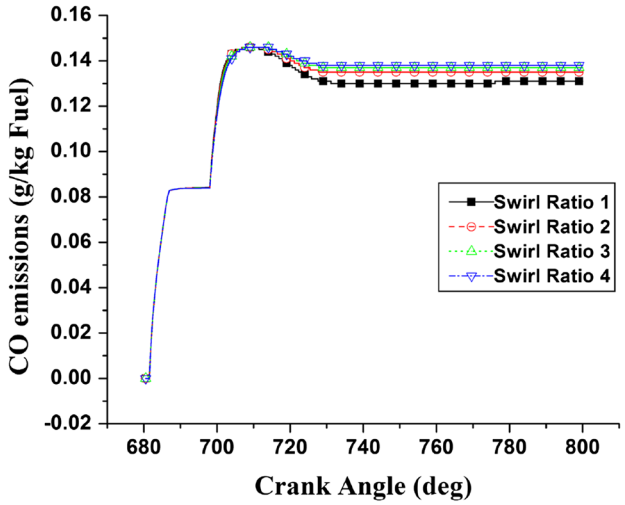

Fig. 7 CO emissions vs. crank angle

decrease in the pressure with increase in swirl intensity. However, the increase in turbulence owing to increased swirl resulted in increased wall heat transfer [20].The effect is illustrated in Fig. 5.

7.2 In-cylinder temperatures

A major amount of turbulence resulted in increased heat loss to the cylinder walls without contributing to the piston wall, but there was a drop in the in-cylinder pressures and temperatures. Figure 6 shows the variation of in-cylinder temperatures with swirl ratio. The increased turbulence in the combustion chamber with swirl ratio facilitates the formation of a well homogeneous mixture, which leads to ideal volumetric combustion causing low-temperature combustion. Increased wall heat transfer losses are the secondary reason for the reduced peak temperatures.

7.3 CO and CO_2 emissions

In-cylinder temperatures play a major role in the formation of emissions. Higher in-cylinder temperatures facilitate the conversion of CO to CO_2 and lower temperatures reduce the formation of NO_x. A clear reduction from 1,206.44 K at swirl ratio 1 to 1,177.26 K at swirl ratio 4 can be seen in Fig. 6. An increase in CO emission with increase in swirl ratio can be observed in Fig. 7. The reduced in-cylinder temperatures and increased wall heat transfer losses with higher swirl ratio do not allow the oxidation reaction of

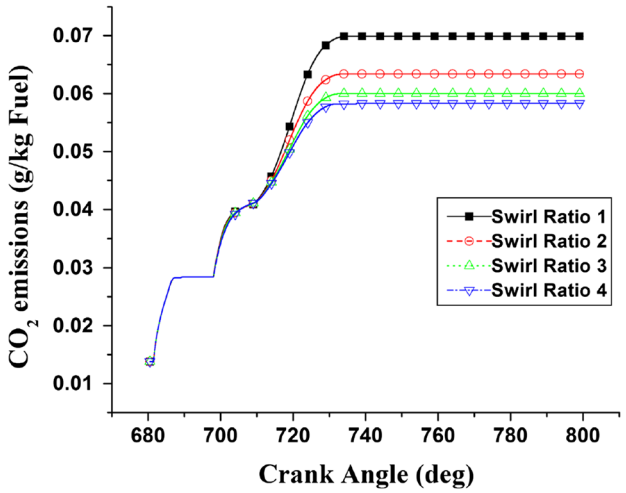

Fig. 8 CO_2 emissions vs. crank angle

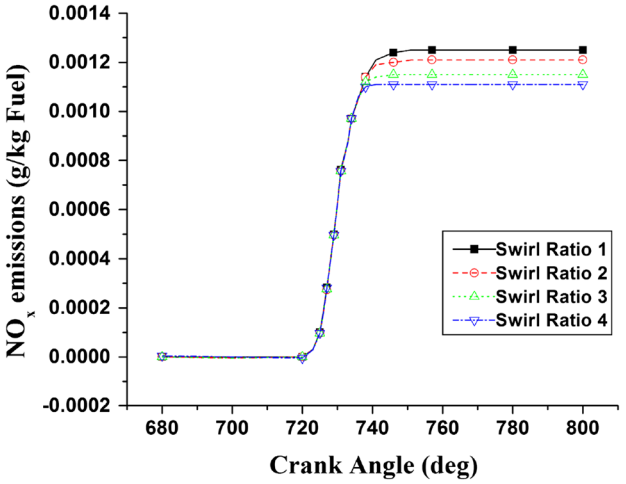

Fig. 9 NO_x emissions vs. crank angle

CO, thus detaining the conversion of CO to CO_2 and resulting in increased CO emissions with swirl ratio [21]. CO_2 emissions variation with crank angle for different swirl ratios can be seen in Fig. 8. A reduction in CO_2 emissions with increase in swirl ratio can be seen in Fig. 8, as the oxidation of CO was not well facilitated because of the reasons mentioned above.

7.4 NO_x emissions

The formation of NO_x is highly dependent on the in-cylinder temperatures, oxygen concentration and residence time for the reaction to take place. As the in-cylinder temperatures do not increase with swirl intensity, significant reduction in NO_x emissions with increase in swirl is obtained [22] as shown in Fig. 9. The reduction in NO_x emission is attributed to the detaining of oxidation of the atmospheric N_2 to react with the available O_2, to form NO_x due to lower cycle temperatures.

7.5 Piston work

Piston work of an IC engine represents the load-bearing capability of the engine. Figure 10 represents the piston work vs crank angle of the HCCI engine under different swirl ratios. The initial decrement in piston work represents the suction and compression strokes (work done on the piston) and the later increase in piston work represents the work done by the piston. A marginal reduction in piston work with increase in swirl ratio can be seen in Fig. 10. It is observed that the improvement in the piston work between the any two consecutive swirl ratios is marginal. However, a maximum variation of 13.3 % at 800 CAD is obtained between swirl ratios 1 and 4. This can be attributed to the

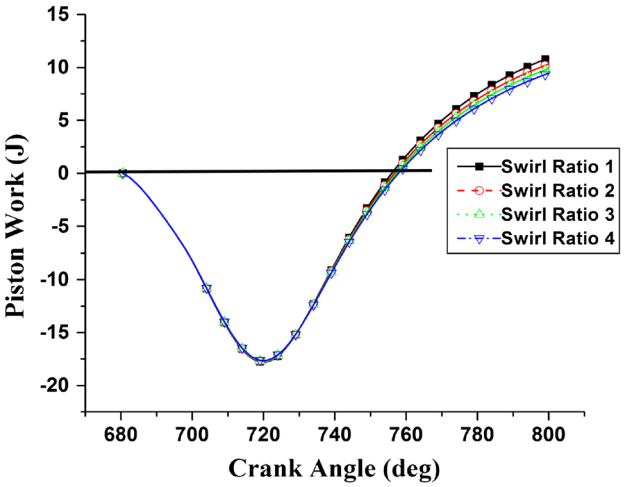

Fig. 10 Piston work vs. crank angle

reduced in-cylinder pressures during the later part of combustion. Thus, reduced pressures reduces the power output.

7.6 Turbulent kinetic energy

Turbulent kinetic energy is an important parameter to determine the burn time and flame speed at a particular region [23]. The turbulence controls the flow dissipation rate, flame propagation rate and heat transfer and it is quantified by turbulent kinetic energy within the cylinder. The regions with low turbulent kinetic energy represents the relatively long time for the flame front to disappear. Turbulent kinetic energy depends on the kinematic viscosity. The kinetic energy of the incoming flow contributes to the turbulent kinetic energy within the cylinder. Figure 11 shows the variation of turbulent kinetic energy with swirl at different

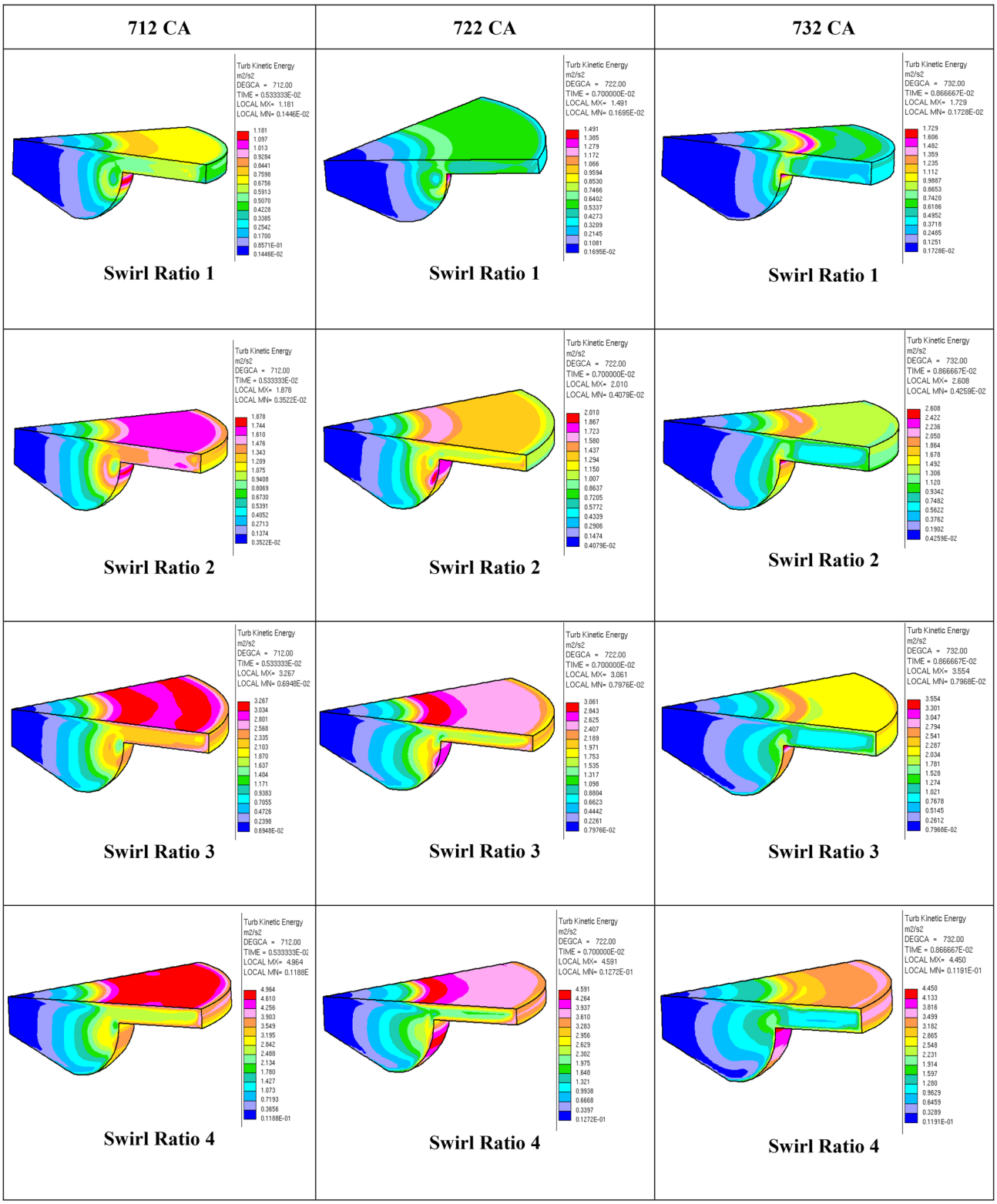

Fig. 11 Variation of turbulent kinetic energy with swirl ratio at various crank angels

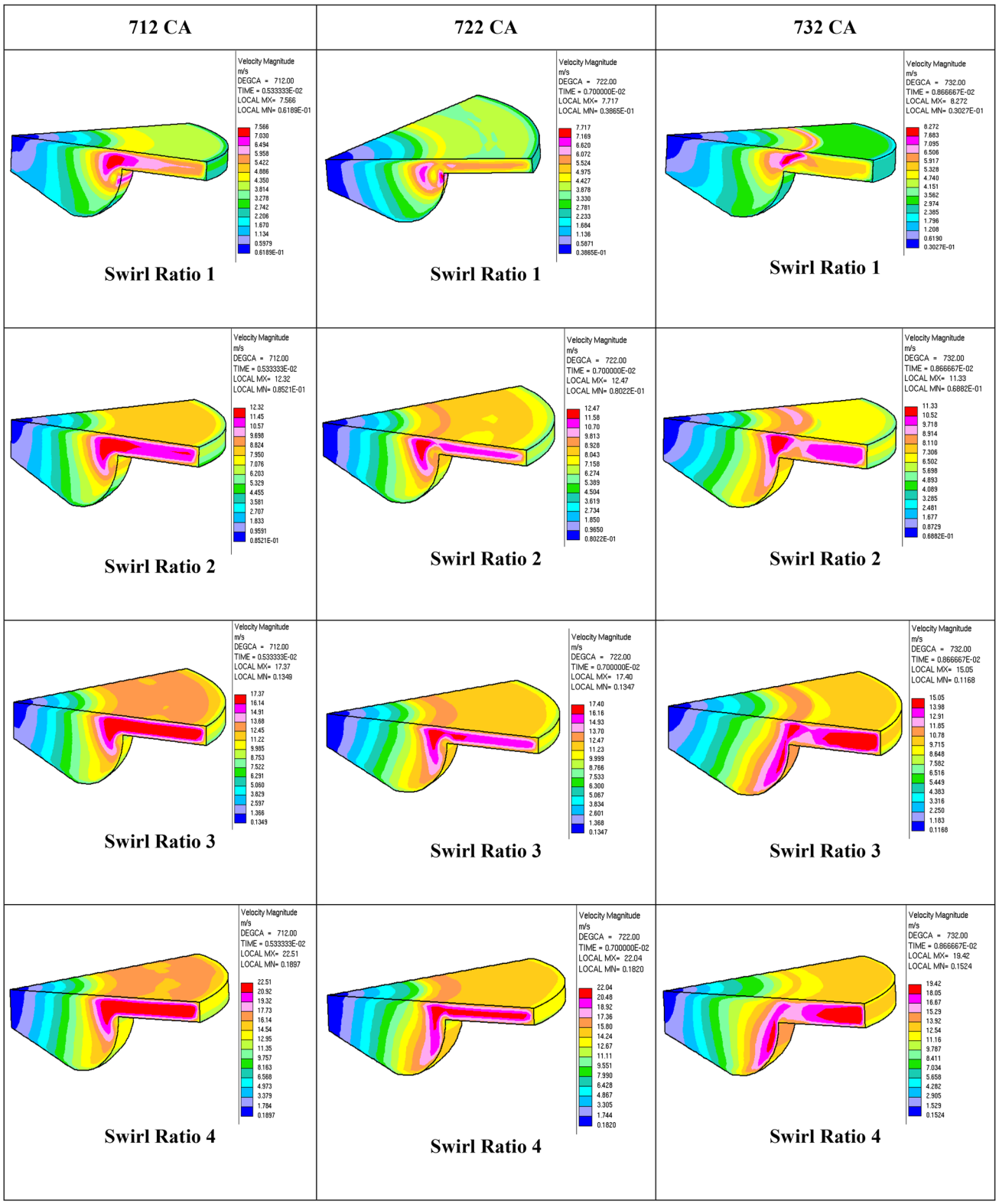

Fig. 12 Variation of velocity magnitude with swirl ratio at various crank angles

crank angles. It is evident from Fig. 11 that the turbulent kinetic energy increases with increase in swirl at all the crank angles. The increase in turbulent kinetic energy is a clear indication of the improved combustion and faster burn time leading toward a perfect volumetric combustion; the important characteristic of HCCI combustion [24]. Also, literature reveals that piston bowl shape is also an important criterion that affects the turbulent kinetic energy. By adopting an altogether different piston bowl geometry, one may achieve higher turbulence. However, adopting higher swirl ratios is cost-effective than using different bowls.

7.7 Velocity magnitude

Velocity magnitude of the combustion chamber gives us a clear idea about the efficient combustion in the combustion chamber. Velocity magnitude of the combustion chamber gives a better idea to locate the regions where incomplete combustion occurs and needs to be improved [25]. The poor velocity regions in combustion volume represent the poor mixing of the fuel and air, leading to incomplete combustion [26]. This shows the need for better combustion chamber designs to create proper turbulence for better mixture formation. Figure 12 shows the velocity magnitude variation at different crank angles for different swirl ratios. It is clear from Fig. 12 that the velocity magnitude increases with swirl ratio, leading to better combustion. The results revealed that better velocity magnitudes representing better combustion can be achieved by increasing the swirl ratio, without modifying the combustion chamber shape.

8 Conclusions

Prediction of engine performance under four swirl ratios has been done using extended coherent flame combustion analysis considering three zones. The present study revealed that ECFM-3Z of STAR-CD well predicted the performance and emissions of the CI engine in the HCCI mode. It was found that swirl ratio is a major factor in achieving the HCCI mode of combustion with significant reduction in harmful NO_x emissions. (volumetric combustion). Marginal reductions in in-cylinder peak pressures were observed with increase in swirl ratio.

This resulted in a reduction in piston work. The reductions in in-cylinder pressures and temperatures are attributed to the increased turbulence within the combustion chamber, resulting in increased wall heat transfer with swirl ratio. It is observed that with the reduction in peak cycle temperatures CO has not been oxidized to CO_2, and thus CO emissions have increased with swirl ratio. Significant reduction in NO_x emission is observed due to reduced in-cylinder temperatures. The reduction in NO_x emissions was achieved by scarifying a little amount of piston work. Increase in swirl ratio resulted in low-temperature combustion, an important characteristic of the HCCI mode combustion. Increased turbulent kinetic energy and velocity magnitude levels within the combustion are achieved with swirl ratio and this could lead to faster burn times. Finally, it can be concluded that higher swirl ratios would achieve volumetric HCCI combustion with better turbulent kinetic energy and velocity magnitude levels, without modifying the combustion chamber geometry.

Acknowledgments The authors would like to thank Dr. Raja Banerjee, Associate Professor from IIT Hyderabad, for allowing us to use the computational facility at IITH, Mr. B. Siva Nageswara Rao from CD-adapco for his support and Mr. P. Madhu, computer lab supervisor, IITH, for his support during the simulation work.

References

1. Epping K, Aceves SM, Bechtold RL, Dec JE (2002) The potential of HCCI combustion for high efficiency and low emissions. SAE Paper No. 2002-01-1923
2. Karthikeya Sharma T, Amba Prasad Rao G, Madhumurthy G (2012) Combustion analysis of ethanol in HCCI engine. Trends Mech Eng 3(1):1–10
3. Duclos JM, Zolver M, Baritaud T (1999) 3D modeling of combustion for DI-SI engines. Oil Gas Sci Technol Rev IFP 54(2):259–264
4. Colin O, Benkenida A (2004) The 3-zone extended coherent flame model (ECFM3Z) for computing premixed/diffusion combustion. Oil Gas Sci Technol Rev IFP 59(6):593–609
5. Ravet F, Abouri D, Zellat M, Duranti S (2008) Advances in combustion modeling in STAR-CD: validation of ECFM CLE-H model to engine analysis. 18th Int. Multidimensional Engine Users' Meeting at the SAE Congress—April, 13 2008, Detroit
6. Subramanian G,Vervish L, Ravet F (2007) New developments in turbulent combustion modeling for engine design: ECFM-CLEH combustion submodel. SAE International—2007-01-0154
7. Huh KY, Gosman AD (1991) A phenomenological model of diesel spray atomization. Proceedings of International Conference on Multiphase flows (ICMF'91), Tsukuba, 24–27 September
8. Bai C, Gosman AD (1995) Development of methodology for spray impingement simulation. SAE Technical Paper Series, SAE Paper No. 950283
9. Reitz RD, Diwakar R (1987) Structure of high-pressure fuel spray. SAE Technical Paper Series, SAE Paper No. 870598
10. Reitz RD, Diwakar R (1986) Effect of drop breakup on fuel sprays. SAE Technical Paper Series, SAE Paper No. 860649
11. Angelberger C, Poinsot T, Delhay B (1997) Improving near-wall combustion and wall heat transfer modeling in si enginecomputations. SAE Technical Paper Series 972881, pp. 113–130
12. Patterson MA, Kong S-C, Hampson GJ, Reitz RD (1994) Modeling the effects of fuel injection characteristics on diesel engine soot and NO_x emissions. SAE Paper 940523
13. Heywood JB (1988) Internal combustion engine fundamentals. McGraw-Hill Company, USA
14. Karlsson A, Magnusson I, Balthasar M, Mauss F (1998) Simulation of soot formation under diesel engine conditions using a detailed kinetic soot model. SAE Technical Paper Series, SAE Paper No. 981022

15. Moureau V, Lartigue G, Sommerer Y, Angelberger C, Colin O, Poinsot T (2005) Numerical methods for unsteady compressible multi-component reacting flows on fixed and moving grids. J Comput Phys 202–2:710–736
16. Pasupathy Venkateswaran S, Nagarajan G (2010) Effects of the re-entrant bowl geometry on a DI turbocharged diesel engine performance and emissions—a CFD approach. J Eng Gas Turbines Power 132:12
17. Zellat M et al. (2005) Towards a universal combustion model in STAR-CD for IC engines: from GDI to HCCI and application to DI Diesel combustion optimization. In: Proceedings of 14th International Multidimensional Engine User's Meeting, SAE Cong
18. Bakhshan Y et al. (2011) Multi-dimensional simulation of n-heptane combustion under hcci engine condition using detailed chemical kinetics. J Engine Res, vol. 22/Spring
19. Ganesh D, Nagarajan G (2010) Homogeneous charge compression ignition (HCCI) combustion of diesel fuel with external mixture formation. Energy 35(1):148–157
20. Viggiano A, Magi V (2012) A comprehensive investigation on the emissions of ethanol HCCI engines. Appl Energy 93:277–287
21. Sjöberg M et al. (2002) GDI HCCI: Effects of injection timing and air swirl on fuel stratification, combustion and emissions formation. No. 2002-01-0106. SAE Technical Paper
22. Zhu Y, Hua Z, Ladommatos N (2003) Computational study of the effects of injection timing, EGR and swirl ratio on a HSDI multi-injection diesel engine emission and performance. No. 2003-01-0346. SAE Technical Paper
23. Yongxian G, Mayor JR, Dahm WJA (2006) Turbulence-augmented minimization of combustion time in mesoscale internal combustion engines. 44th AIAA aerospace sciences meeting and exhibit, AIAA-2006-1350
24. Chmela, FG, Gerhard CO (1999) Rate of heat release prediction for direct injection diesel engines based on purely mixing controlled combustion. No. 1999-01-018, SAE Technical Paper
25. Krishna BM, Mallikarjuna JM (2011) Effect of engine speed on in-cylinder tumble flows in a motored internal combustion engine—an experimental investigation using particle image velocimetry. J Appl Fluid Mech 4(1):1–14
26. Goryntsev D et al (2009) Large eddy simulation based analysis of the effects of cycle-to-cycle variations on air–fuel mixing in realistic DISI IC-engines. Proc Combust Inst 32(2):2759–2766